Journal of The Electrochemical Society, **149** (8) H146-H152 (2002)
0013-4651/2002/149(8)/H146/7/$7.00 © The Electrochemical Society, Inc.

Electrostatic Actuators with Intrinsic Stress Gradient

II. Performance and Modeling

Anil K. Chinthakindi* **and Paul A. Kohl****,z**

School of Chemical Engineering, Georgia Institute of Technology, Atlanta, Georgia 30332-0100, USA

Electrostatic actuators are used as voltage-controlled oscillators or resonators in high frequency applications. The change in deflection of a cantilever beam due to an applied voltage leads to change in capacitance between the plates of the beam. However, the range of operation of these devices is limited due to the nonlinear nature of the applied electrostatic forces as the cantilever beam moves. The pull-down instability of the beam limits the travel distance of elastically suspended parallel-plate electrostatic actuators to about one-third of the initial gap distance. The movement of curved actuators under application of an electrostatic force is investigated. The initial curvature of the movable electrode was established by using a built-in stress gradient in the metallic cantilever-beam. A two-dimensional, semi-analytical, finite difference model was used to simulate the behavior of the devices. Three-dimensional modeling was also performed to understand the movement of the cantilever beams. The pull-down voltage of the beams was studied as a function of initial tip deflection, shape of the movable electrode, and anchor type. The stable range of operation of these cantilever beams before pull-down was found to be smaller than one third of the tip deflection. After pull-down, the movable electrode was found to ''uncurl'' upon further application of voltage. This was attributed to the higher order curvature of the movable electrode with large built-in stress gradient.
 [DOI: 10.1149/1.1486455]

Manuscript submitted July 19, 2001; revised manuscript received February 10, 2002. Available electronically June 14, 2002.

Microelectromechanical systems (MEMS) is a technology which leverages the existing state-of-the art integrated circuit (IC) fabrication technology and enables the batch fabrication of miniature mechanical structures, devices, and systems.[1-5] This technology exhibits its advantages such as cost reduction through batch fabrication, device-to-device consistency, and performance advancements from dimensional downscaling leading to size and weight reduction. Several MEMS devices, which have been successfully commercialized, include microsensors, micro-optics, pressure sensors, accelerometers, and ink-jet nozzles.[2-4] Emerging applications for MEMS are in the areas of optics, microfluidics, and wireless communications.[2]

Most of the MEMS designs use electrostatic, piezoelectric, thermal, pneumatic, or magnetic actuation to move the micromachined parts.[2,3] Due to the availability of large electrostatic forces and high energy densities, electrostatic actuation has advantages as compared to other actuation mechanisms. In most electrostatic actuators, the balance between the electrostatic force and the mechanical restoring force controls the deflection of the electrodes. Upon application of the voltage, a continuous movement of the electrodes is desirable for tuning applications.[6-10] Unfortunately, the range of continuous motion of the electrostatically actuated beam is limited due to the presence of nonlinear electrostatic forces. This leads to the well-known ''pull-down'' instability in these devices, which prevents the stable positioning of the electrodes over the gap distance.

The pull-down voltage instability was first observed by Nathanson *et al.*[7] in 1967. When the applied voltage is increased beyond a critical value, there is no longer a steady-state configuration of the electrostatically actuated devices. This instability severely restricts the range of motion of these devices and limits the continuous tuning range of the electrostatic actuators. In order to illustrate this phenomenon, a one-dimensional lumped parameter model can be used. One can consider the system shown in Fig. 1 consisting of two parallel-plate electrodes separated by a gap distance, d, with one plate fixed and the other suspended by an elastic restoring force, kx, where k is the linear spring constant and x, the displacement of the top electrode. If a voltage, V, is applied across the plates, the resulting attractive electrostatic force, F_e, neglecting the fringing effects, is given by Eq. 1

$$F_e = \frac{1}{2}\frac{\varepsilon_o A V^2}{(d-x)^2} \quad [1]$$

where A is the area of the movable plate, d is the initial gap distance, and ε_0 is the permittivity of free space. The electrostatic force is nonlinear, since it is directly proportional to $1/(d-x)^2$ and the square of the applied voltage. However, the elastic restoring force is directly proportional to x. The total upward force on the movable (top) plate is given by Eq. 2

$$F(x) = kx - \frac{1}{2}\frac{\varepsilon_o A V^2}{(d-x)^2} \quad [2]$$

In static equilibrium, $F(x) = 0$, and for the static equilibrium to be stable, $\partial F/\partial x$ must be less than zero. At the brink of instability, $\partial F/\partial x = 0$.

Using these two conditions the instability occurs at $x = d/3$ and the pull-down voltage is given by $V_{\text{pull-down}} = [(8kd^3)/(27\varepsilon_o A)]^{1/2}$.

The results of the lumped parameter modeling show that the parallel-plate electrostatic actuator operates in a stable region at voltages below the critical voltage, $V_{\text{pull-down}}$. The movable beam is unstable for all voltages greater than the critical pull-down voltage, $V_{\text{pull-down}}$. A beam with a different restoring force, say kx^2, would remain in the stable region until the beam reaches half the initial gap distance. For a hypothetical restoring force of kx^n, the operating region would be from d to $nd/(n+2)$.

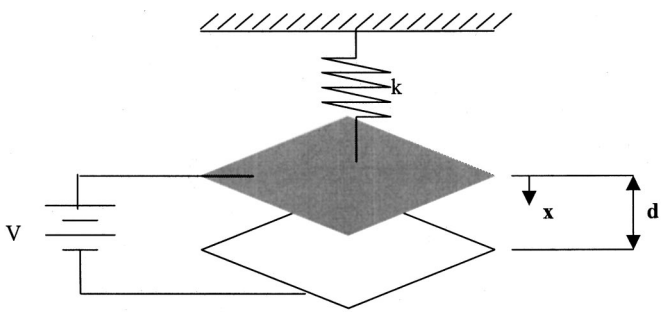

Figure 1. A schematic diagram of the lumped model with parallel electrodes.

* Electrochemical Society Student Member.
** Electrochemical Society Active Member.
z E-mail: paul.kohl@che.gatech.edu

A strain-stiffening method has been proposed by Hung and *et al.*[10,11] to extend the travel range of analog tuned electrostatic actuators. As the beam deflects with the application of voltage, the tensile stress in the beam increases due to increasing strain in the beam. This increase in stiffness tends to increase the range of operation of the device. In first order, the strain-stiffening term can be viewed as a cubic spring constant term (kx^3). For larger deflections, the strain-stiffening effect can dominate over the linear elastic restoring forces (kx), leading to a stable operating region from d to $3d/5$. The effectiveness of the strain-stiffening effect depends on the residual stress in the beam. If the beam is tension-dominated due to residual stress, the strain-stiffening effect is reduced since the increase in stress due to deflection is small compared to the initial residual stress.[10]

''Leveraged bending'' is another technique proposed by Hung and Senturia [10,11] to increase the travel range of the actuators. By applying an electrostatic force to only a portion of a structure, the remaining portion of the structure acts as a lever and can be actuated through the entire gap distance between the electrodes. In this technique, the bottom electrode is positioned near the beam supports, and the bottom electrode covers only part of the area of the upper beam. The actuated portion of the beam moves by about one-third of the gap distance, while the unactuated portion of the beam moves through a greater portion of the gap distance. The extended tunability comes at the cost of increased actuation voltage. Similar to the strain-stiffening effect, the residual tensile stress in the beam has a negative effect on the travel range for the leveraged bending technique.[10]

The stable behavior of the electrostatic actuator can also be improved by incorporating curvature to the electrodes. Legtenberg *et al.*[12] have shown that the pull-down behavior of the curved electrostatic actuator depends on the shape of the curved electrode. Stable behavior with relatively large displacements and forces can be generated by curved electrodes where curvature with length can be described by a polynomial order greater than 2. The beam deflection of the movable electrode becomes constrained by the curved electrode geometry before electrostatic pull-down can occur.[13] This results in a larger stable region of operation.

A MEMS variable capacitor with a curved movable electrode and a planar fixed electrode is considered in this study. Previously, it has been shown that the initial curvature of the movable electrode can be controlled by varying the deposition conditions. The movable (top) electrode was made of gold and had an initial curvature due to the intrinsic stress gradient incorporated in the beam during the deposition process.[14] A polymer dielectric material separated the top electrode from the bottom electrode, which was made of aluminum. The goal of this study was to investigate the voltage-deflection behavior of five electrostatic actuators with different shapes. The effect of initial deflection, curvature, and shape of the movable electrode on the electrostatic behavior of the device was studied. 2D, semianalytical modeling was performed to analyze the behavior of the full-hinged, square-shaped actuator. The 2D semianalytical model provided physical insight into the behavior of the device. Further, 3D finite element modeling using MEMCAD (Coventor, Inc.) was performed to understand the voltage *vs.* 3D deflection of the devices.

Theory

The movable electrode of the electrostatic actuator was modeled as a cantilever beam, with the dimensions of length L, width w, and thickness t. The beam was assumed to be fully clamped at one end and free at the other end. The stationary electrode covered the full area under the movable electrode. The initial curvature of the movable electrode was modeled by providing the beam with a tensile stress gradient. The stress gradient was physically incorporated in the beam during the formation of the cantilever beam. A model for calculating the deflection of the beam after release due to relief of the residual stress was presented in Part I of this study.[14]

The initial curvature of the cantilever beam with a built-in stress gradient can also be modeled by assuming the beam to be made of two different materials.[13] An internal stress gradient can be created by using two materials with dissimilar coefficient of thermal expansion (CTE). Due to the mismatch between the CTE of the two materials, the cantilever beam can be made to deflect away from its original position in the positive (upward) or in the negative (downward) direction by changing the temperature. The theory for modeling the beam using this approach is presented here and used to model the electrostatic movement of the cantilever beam.

The change in radius of curvature of a bimetallic cantilever beam would be the same as that of a freestanding bimetallic strip of twice the length of the cantilever beam. Assuming that the bimetallic beam is planar (flat) at room temperature, the final radius of curvature of the freestanding film can be calculated. If there are no external forces acting on the bimetallic strip, then Eq. 3

$$P_1 = P_2 = P \quad \text{(equilibrium)} \tag{3}$$

Due to the CTE mismatch, the strain developed in the two materials must be equal at the boundary, which leads to Eq. 4

$$\alpha_1(\Delta T) + \frac{P}{E_1(wt_1)} + \frac{t_1}{2\rho} = \alpha_2(\Delta T) - \frac{P}{E_2(wt_2)} - \frac{t_2}{2\rho} \tag{4}$$

Where E_1 and E_2 are the biaxial modulus, α_1 and α_2 are the CTEs of material of two layers, and ΔT is the change in temperature, P_1 and P_2 are the external forces applied on layer 1 and 2, respectively, and ρ is the radius of curvature of the bimetallic strip. The moment of inertia of the top layer, I_1, is given by $(wt_1^3/12)$, and the moment of inertia of the bottom layer, I_2, is given by $(wt_2^3/12)$, where w is the width of the cantilever beam, and t_1 and t_2 are the thickness of the top and bottom layers, respectively. Solving for force, P using Eq. 4 yields Eq. 5

$$P = E_2 t_2 w\left[\frac{\Delta\alpha\Delta T - (t_1 + t_2)/(2\rho)}{1 + (E_2t_2)/(E_1t_1)}\right] \tag{5}$$

The bending moment, M is generated by the reaction forces P_r, which have the same magnitude as force P but are in the opposite direction. The moment, M, when calculated from stress fields yields Eq. 6[13]

$$M = |P_r|\left(\frac{t_1 + t_2}{2}\right) = \frac{E_1I_1 + E_2I_2}{\rho} - P\left(\frac{t_1 + t_2}{2}\right) \tag{6}$$

Substituting the expressions for P from Eq. 5, and for the beam with initial radius of curvature of ρ_o, the change in radius of curvature is given by Eq. 7

$$\frac{1}{\rho} - \frac{1}{\rho_o} = \frac{(\alpha_2 - \alpha_1)(\Delta T)}{\frac{t_1}{2}\left[\frac{\left(1 + \frac{E_2I_2}{E_1I_1}\right)\left(1 + \frac{E_2t_2}{E_1t_1}\right)}{6\frac{E_2}{E_1}\frac{t_2}{t_1}\left(1 + \frac{t_2}{t_1}\right)} + \left(1 + \frac{t_2}{t_1}\right)\right]} \tag{7}$$

The initial deflection of the bimetallic cantilever beam along the length, $H(x)$ is given by Eq. 8

$$H(x) = \frac{x^2}{2}\left(\frac{1}{\rho} - \frac{1}{\rho_o}\right) \tag{8}$$

Thus, the initial deflection of the curved actuator can be modeled if the thickness, elastic modulus, and CTE of the materials are known.

The electrostatic force acting on the movable electrode is given by $F = (\varepsilon AV^2/2g^2)$, where ε is the permittivity of the medium, A is the area of the electrodes, V is the applied voltage, g is the gap distance between the two electrodes, which is equal to the sum of

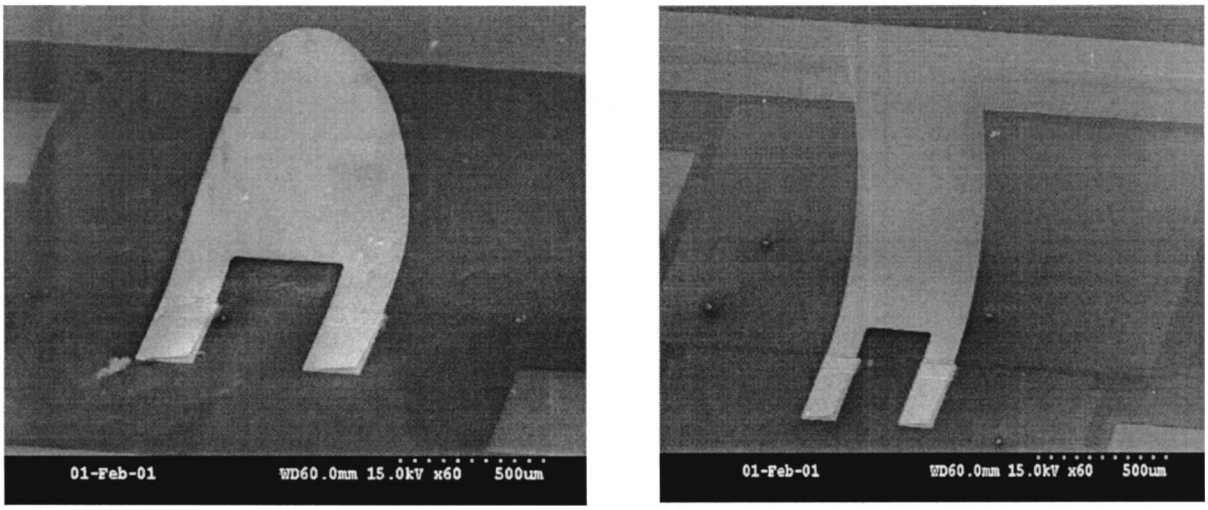

Figure 2. Scanning electron microscopy images of (a, left) double-hinged elliptical actuator and (b, right) double-hinged rectangular actuator.

initial gap distance H and displacement y. The force per unit length acting on the cantilever beam is $(\varepsilon V^2/2g^2) \times w$. From continuum mechanics

$$EI\frac{d^4y}{dx^4} = -\frac{V^2\varepsilon b}{2(y+H)^2} \quad [9]$$

where EI is the flexural rigidity of the beam, and H is the initial height of the beam as a function of distance, x, along the length of the beam. $H(x)$ can be obtained either by using the stress gradient model[14] or by approximating the beam by a bimetal composite and matching the initial deflection, as outlined above. Equation 9 is a fourth-order nonlinear differential equation, which can be solved with the following boundary conditions

1. $y(x = 0) = 0$ No deflection at the clamped end.
2. $dy/dx\,(x = 0) = 0$ Slope of the deflection at the clamped end is zero.
3. $d^2y/dx^2\,(x = L) = 0$ No moment acting on the free end.
4. $d^3y/dx^3\,(x = L) = 0$ No Shear force acting on the free end.

The differential equation is solved numerically by employing finite difference techniques. The deflection of the beam has been calculated at five different points along the cantilever beam length. The capacitance between the top and the bottom plate is given by Eq. 10

$$C = \int_0^L \frac{\varepsilon_0 w dx}{(g_{\text{air}} + (1/k)\, g_{\text{dielectric}})} \quad [10]$$

Where g_{air} is the gap between the plates with air as the dielectric medium, k is the relative permittivity of the dielectric material, and $g_{\text{dielectric}}$ is the thickness of the dielectric medium. Equation 10 was numerically integrated to determine the capacitance of the device.

Experimental

Detailed process sequence for the fabrication of the electrostatic actuators was presented previously in Part I of this study.[14] In summary, 400 nm of aluminum was deposited using a dc magnetron sputterer (CVC products) and patterned to form the fixed (bottom) electrodes. 1.6 μm of polymeric material was used as the dielectric material between the electrodes. The dielectric polymer was then patterned to form contact vias. 1.5 μm of photoresist (Shipley Chemical Co. 1800 series) was deposited on the wafer and patterned to open the cantilever beam anchor regions. 30 nm of titanium followed by 1 μm of gold was deposited using electron-beam evaporation (CVC products) and patterned to form the cantilever anchor regions. The gold and titanium layers were then chemically etched. Photoresist was spun on the wafer to form a 1.5 μm film to be used as the release layer. Titanium (30 nm) followed by 200 nm of gold was deposited on top of the photoresist to form the seed layer for electroplating. 2 μm of soft gold was electrochemically deposited at a current density of 3 mA/cm^2 at 60°C from a pH 7 gold plating bath.[15] Hard gold thicknesses of 100-200 nm were electroplated on the soft gold layer at a current density of 5 mA/cm^2 at room temperature using a cobalt-hardened gold plating bath to provide a tensile stress.[14] The gold layer was patterned to form the top electrode using conventional lithographic techniques. The cantilever beams were released by dissolving the photoresist in acetone. The stiction during release was reduced by treating the gold cantilever beams with an alkane thiol solution to form a hydrophobic self assembled monolayer (SAM) on the gold.[14] The SAM was formed by soaking the released beams in a 1 mM solution of dodecyl thiol in absolute ethanol solution.

Electrostatic actuators with different shapes and anchor attachments were analyzed in this study. A low-temperature, vacuum microprobe station (MMR Technologies) was used to investigate the deflection of these devices with applied voltage. The probe station enabled testing of the devices at temperatures between 77 and 373 K by use of a resistive heater and a Joule-Thompson cooler. Testing was performed between 100 Pa and 100 kPa absolute pressure. The cantilever deflection was measured using a high-resolution microscope.

Results

The goal of this study was to investigate the voltage-deflection behavior of the curved electrostatic actuators fabricated using the stress gradient approach. The initial curvature of the movable electrode was controlled by varying the thickness of the hard gold deposited on top of the electroplated soft gold. Scanning electron microscopy (SEM) images of the electrostatic actuators fabricated using this approach are shown in Fig. 2. A double-hinged elliptical and double-hinged rectangular-shaped actuators are shown in Fig. 2a and 2b, respectively. The movable electrode in the actuators was 2.5 μm thick and composed of 2.3 μm soft gold and 0.2 μm hard gold.

Figure 3 shows the dimensions of the electrode shapes investigated in this study: (a) full hinged square, (b) full hinged semicircle, (c) double-hinged square, (d) double-hinged half ellipse, and (e) double-hinged rectangular shapes of the movable electrode. The

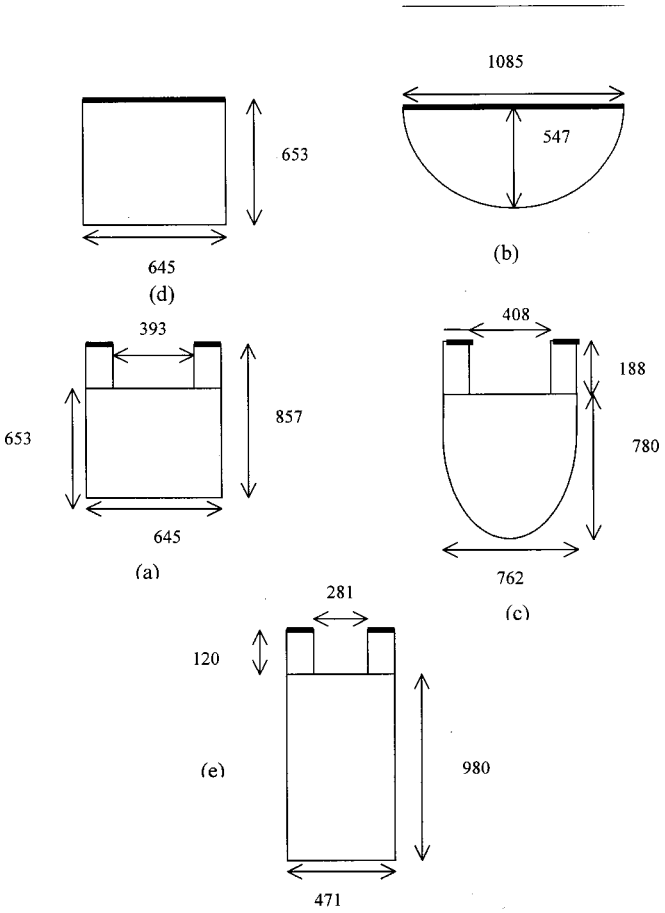

Figure 3. Dimensions and shapes of top electrodes of actuators (a) full-hinged square, (b) full-hinged semicircle, (c) double-hinged square, (d) double-hinged ellipse, and (e) double-hinged long rectangle.

dark regions in Fig. 3 show the anchor areas for each of the actuators. The total surface area of the electrodes in Fig. 3 are all the same, resulting in a similar net force applied to each of the electrodes at a given voltage. For each of these cantilever beams, the stationary electrode covered the full area under the movable electrode. Each of the five devices in Fig. 3 was tested to evaluate the effect of initial tip deflection, anchor type, and shape of the top movable electrode.

Figure 4 shows the pull-down behavior of the actuator with double-hinged square electrode shown in Fig. 3a. The movable electrode was comprised of 0.1 μm of hard gold over 2.3 μm of soft gold. The initial tip deflection of the movable electrode was 206 ± 5 μm (zero applied voltage). At 70 V, the double-hinge square electrode was pulled down and made physical contact with the bottom dielectric. The solid line in Fig. 4 shows the 3D modeling results. The pull-down voltage calculated by the 3D model was 77.25 V. A 3D image of the device model for the double-hinge square actuator obtained using MEMCAD is shown in Fig. 5. A stress gradient of 20 MPa/μm over the thickness of the movable electrode gave an initial tip deflection of 200 μm. The curvature produced by the 3D model was similar to the actual curvature of the movable electrode.

Figure 6 shows the measured tip-deflection *vs.* applied voltage for the actuator with a semicircular shaped movable electrode, fully clamped at one end, Fig. 3b. The tip deflection of the movable electrode at 0 V was 101 ± 5 μm. Continuous deflection of the beam occurred up to a voltage of 100 V. At 100 V, the tip deflection of the movable electrode was 95 ± 5 μm. The beam was pulled down in contact with the dielectric material at a voltage of 125 V. The center portion of the beam was in contact with the lower dielectric, however, the tip was still raised 25 ± 5 μm above the dielectric. That is, the center portion of the beam touched down but not the tip. The solid line in the plot shows the modeled tip deflection *vs.* applied voltage. The pull-down voltage as predicted by MEMCAD modeling was 113.25 V.

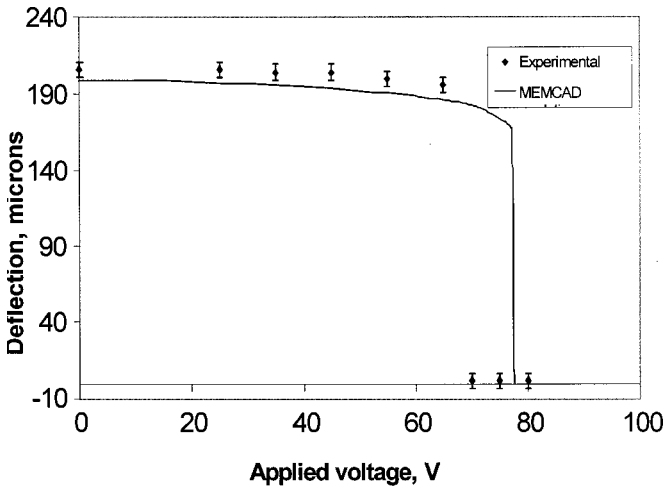

Figure 4. Tip deflection *vs.* voltage of double-hinged square actuator.

The behavior of the actuator with the double-hinged elliptical electrode (Fig. 3c) with an intrinsic stress gradient greater than the previous two cantilevers was then investigated. Figure 7 shows the tip-deflection *vs.* voltage for the double-hinged elliptical actuator. The initial tip deflection was 245 ± 5 μm. The tip deflection of the elliptical beam changed gradually from 0 to 70 V, as shown in Fig. 7. When the voltage was increased to 75 V, the elliptical beam was partially pulled down and touched in the center of the beam, resulting in a tip deflection of 150 ± 5 μm. As the voltage was further increased to 80 V, the beam further uncurled and had a tip deflection of 75 ± 5 μm. The elliptical beam was pulled down flat at 85 V. A stress gradient of 40 MPa/μm was used to model the elliptical beam. The 3D MEMCAD model predicted that the elliptical beam should remain stable from 0 to 86 V followed by pull-down at 86.5 V.

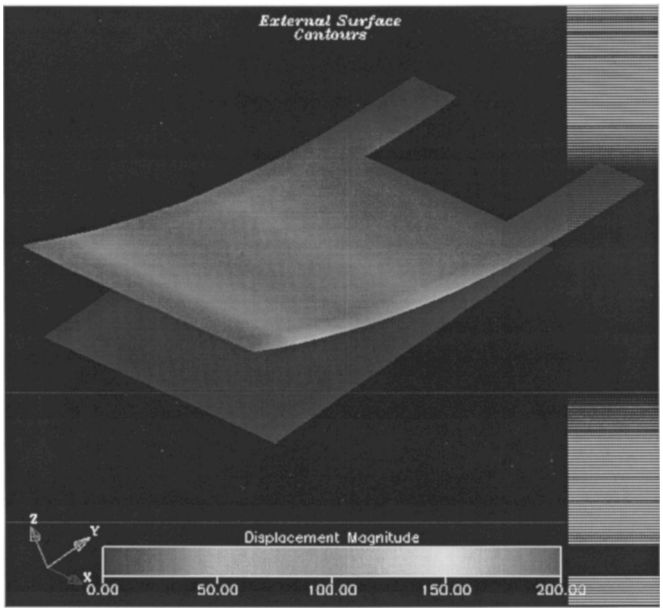

Figure 5. 3D model of the actuator generated using MEMCAD.

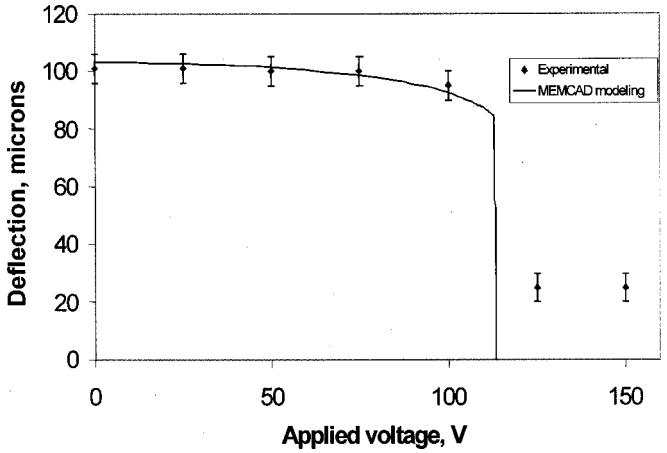

Figure 6. Tip-deflection *vs.* voltage of variable capacitor with semicircular top electrode hinged along one side.

The measured tip-deflection *vs.* voltage of the full-hinged square-shaped actuator (Fig. 3d) is shown in Fig. 8. The initial tip deflection of the beam was 136 ± 5 μm. As the voltage was increased to 50 V, the tip deflection of the beam decreased to 129 ± 5 μm. The middle portion of the beam touched down at 65 V. At 65 V the beam tip was 68 ± 5 μm above the dielectric. At higher applied voltages, the beam smoothly uncurled to a deflection of 52 ± 5 μm before snapping down. The analysis of this device indicates that the initial curvature of the movable electrode deviated from the second-order polynomial relationship. Once the beam touched in the center, the remaining length of the beam was stiffer, leading to higher pull-down voltages prior to complete snap-down. The dashed lines in the graph show the 2D finite difference modeling of this device. The calculated value of the pull-down voltage was 62 V compared to the experimental value of 65 V. It was observed that at 65 V, the remaining movable portion of the electrode had an active length of 40% of the original length of the actuator. 2D analysis was performed on the cantilever beam with this reduced length, which was assumed to be fixed at one end (for calculation purposes), so the deflection could occur only at the free end. The radius of curvature of the reduced length beam was assumed to be the same as that of the full-length cantilever beam. This gave a calculated tip deflection of 64 μm at the partial pull-down point compared to the actual value of 68 μm. The predicted value of second pull-down voltage (reduced length) was 105 V.

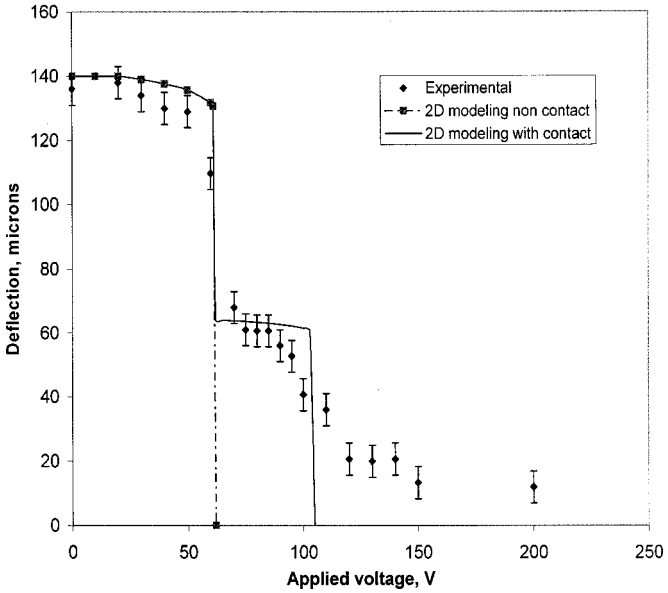

Figure 8. Tip deflection *vs.* voltage of full-hinged square actuator.

Figure 9 shows the calculated value of capacitance of the device in Fig. 8 as a function of voltage. The solid line shows the capacitance *vs.* applied voltage obtained from the two-step pull-down voltage analysis. The initial capacitance of the device is 0.4 pF and increased to 0.53 pF at 60 V. The capacitance increased to 3.74 pF at first snap-down. The capacitance smoothly changed to 3.93 pF at 100 V followed by a maximum capacitance of 5.6 pF.

A double-hinged rectangular actuator was subjected to similar voltage application and the corresponding tip deflection is plotted in Fig. 10. As the applied voltage was increased, it can be seen that the beam snapped down similar to the full hinged square device. The beam had an initial tip deflection of 175 ± 5 μm and was pulled down at a voltage of 40 V, leading to second stable region. The tip

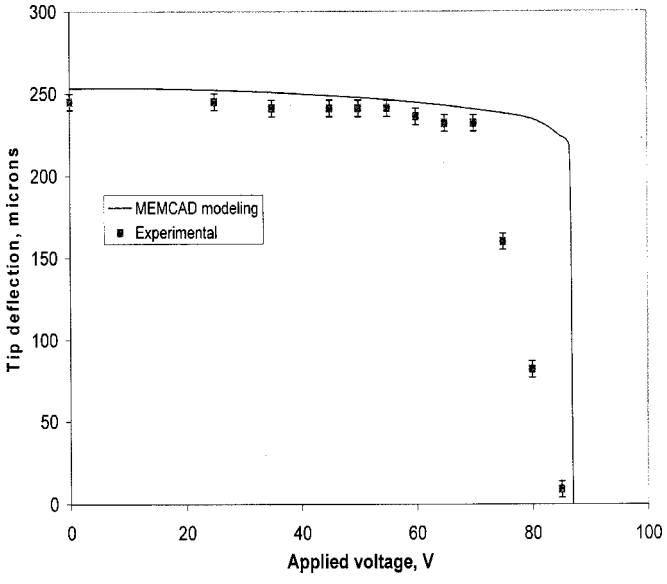

Figure 7. Tip deflection *vs.* voltage of double-hinged elliptical actuator.

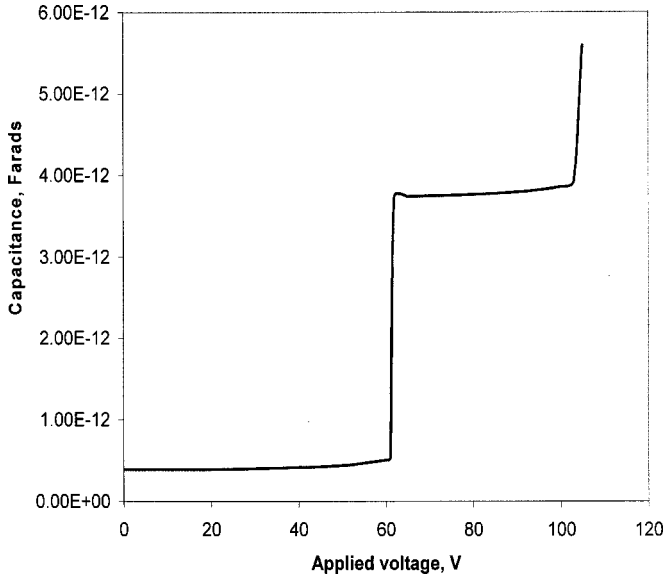

Figure 9. Calculated value of capacitance *vs.* voltage of full-hinged square actuator.

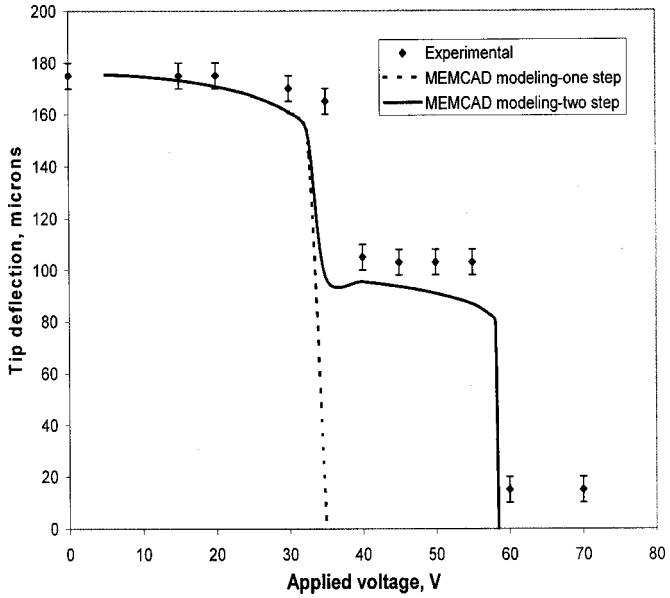

Figure 10. Tip deflection *vs.* voltage of double-hinged long rectangular actuator.

deflection of the device at 40 V was 105 ± 5 μm. The movable electrode snapped down to its final state at 60 V. 3D MEMCAD analysis (dashed lines) gave a pull-down voltage of 35 V. The length of the movable portion was observed to be 70% of the full beam length. Using this reduced length as the "new" cantilever beam, the second pull-down voltage was calculated to be 58.5 V compared to the observed value of 60 V.

The results of the electrostatic analysis of the five actuators are summarized in Table I. The shape of the electrode (square, semicircular, elliptical, or rectangular), dimensions of the movable electrode (length *x* width), type of anchor attachment (full hinge or partial double hinge), and the initial tip deflection are presented *vs.* the pull-down voltage for each actuators. For the beams with two-step snap-down, only the first pull-down voltage is presented.

Discussion

The pull-down voltage of the curved electrostatic actuator was found to be a strong function of initial curvature, anchor attachment, and shape of the movable electrode. The initial deflection and curvature of the movable electrode was controlled by varying the built-in stress gradient in the gold film. As calculated by the models, these devices exhibited continuous movement with applied voltage before being pulled down to the bottom dielectric material.

The tip deflection of the movable electrode was dependent on the shape of the cantilever beam. The electrodes were fabricated with curved or straight edges. Due to the built-in stress gradient in the beam, the movable electrode with rectangular and square front shapes resulted in corner regions with greater deflection than the center of the front edge of the beam. The two corners of the beam had approximately equal deflection. The extra curvature at the corners was due to the stress concentration at the corner regions of the beam. The movable electrode with elliptical and semicircular shapes had smooth curvatures along their length without corner effects. These electrodes showed uniform deflection where the tip of the electrode always had the greatest deflection. The electrostatic actuators with the curved fronts were found to be more reproducible in shape and performance than the square-edged devices.

Table I. Summary of the pull-down behavior of the electrostatic actuators.

Sl. no.	Shape	Dimensions (μm)	Anchor type	Tip deflection (μm)	Pull-down voltage (V)
1	Square	857 × 645	Partial	200	70
2	Semicircle	547 × 1085	Full	100	125
3	Elliptical	968 × 762	Partial	250	85
4	Square	653 × 645	Full	135	60
5	Rectangle	1100 × 471	Partial	175	70

The electrostatic behavior of the actuators with a short (and wide) movable electrode was compared to the actuators with long (and narrow) movable electrode (area was held constant). The pull-down behavior of double-hinged square electrodes can be compared to the double-hinged long rectangular electrodes (Table I). The dimensions of the double-hinged square electrode are 857 × 645 μm and the dimensions of the double-hinged rectangular electrode are 1100 × 471 μm. The two beams had approximately the same initial tip deflection (200 μm *vs.* 175 μm). By changing the shape from square to rectangular, the pull-down voltage of the top electrode was reduced from 70 to 40 V, which corresponds to 43% reduction in pull-down voltage. Similarly, by comparing the behavior of the full-hinged semicircular device to a full-hinged square device, it can be seen that they had comparable tip deflections (100 *vs.* 135 μm). A 52% reduction (from 125 to 60 V) in pull-down voltage was achieved by making the beam longer and narrower. The full-hinged semicircular top electrode had greater flexural rigidity than the full hinged square electrode. The flexural rigidity of the beam is given by $(E \times I)_{\text{beam}}$, where E is the biaxial elastic modulus of the material and I is the moment of inertia. The moment of inertia of the beam was reduced as the beam became longer (and narrower), thereby reducing the rigidity of the structure.

The pull-down voltage of the electrostatic actuator was found to be directly proportional to the initial tip deflection of the movable electrode. The greater the distance between the two electrodes, the greater is the electrostatic force required to move the structure. This can be shown by comparing the pull-down behavior of the double-hinged elliptical electrode and the double-hinged (long) rectangular electrode (Table I). The tip deflection of the long rectangular electrode was 175 μm (0.1 μm of hard gold over 2.3 μm of soft gold). The elliptical electrode had an initial tip deflection of 250 μm (0.2 μm of hard gold over 2.3 μm of soft gold). This resulted in an increase in the pull-down voltage from 40 to 85 V (an increase of 112%), for corresponding tip deflections of 175 and 250 μm (43% increase). Even though the length of the beam was shortened from 1100 to 968 μm (a 12% decrease), this effect was smaller than the tip deflection effect.

Partial anchoring of the movable electrode reduced the flexural rigidity of the beam, which resulted in lower pull-down voltages. This can be shown by comparing the electrostatic behavior of the full-hinged square actuator *vs.* the double-hinged square actuator. Even though the tip deflection of the double-hinged square electrode was more than the full-hinged square electrode (200 *vs.* 135 μm), the pull-down voltage increased only by 10 V (from 60 to 70 V). This was due to the partial anchoring of the double-hinged square electrode. The partial (or double) hinge covered 40% of the width of the movable electrode and reduced the rigidity of the structure.

The pull-down behavior of the curved electrostatic actuators was a strong function of the initial curvature of the electrodes. It was shown by Legtenberg *et al.*[12] that the second derivative of the total potential energy with respect to polynomial order, n, is negative for $n \leqslant 2$, indicating unstable behavior. The actuators with movable electrodes created by deposition of 0.1 μm of hard gold showed an initial curvature of polynomial order 2. These devices showed distinct regions of stable and unstable behavior. This indicates that the stress gradient model developed is appropriate for beams with small intrinsic stress gradients (20 MPa/μm).[14]

It was observed that as the length of the beam increases, the second-order polynomial description of the beam curvature becomes less accurate and deviations from the stress gradient model become more severe.[14] The movable electrodes with large intrinsic stress

gradients created by the deposition of 0.2 and 0.3 μm of hard gold have shown an initial curvature of polynomial order greater than 2. The hard gold thickness variation along the length of the movable electrode during electroplating would result in nonuniform stress gradient along the length leading to the curved beam with higher order curvature. These devices have shown partial snap-down leading to an ''uncurling'' of the devices upon application of voltages greater than critical pull-in voltage. Similar results with step-like unstable and stable regions were obtained by Legtenberg *et al.* for electrostatic curved electrode actuators.[12] It has been shown that for the electrodes with curvature of order greater than 2, the second derivative of potential energy with respect to the polynomial order becomes positive, indicating stable behavior. The curved beam uncurls along the fixed electrode as the voltage is increased, leading to stable behavior (no pull-in) up to the maximum tip deflection. This behavior of the beams with higher order of initial curvature is attributed to the constrained beam deflection involving contact mechanics. The imperfections at the surface of the top and bottom electrode also aid in the partial snap-down of the movable electrode. Surface asperities, entrapped particles, or residues between the electrodes after the fabrication process could act like small bumpers, preventing the beam from complete snap-down.

Conclusions

The voltage-deflection behavior of the electrostatic actuators with intrinsic stress gradient was studied. The electrostatic behavior of the actuator was found to be strong function of initial tip deflection, type of anchor attachment, and shape of the movable electrode. The pull-down voltage of the actuator with long and partially anchored movable electrode was found to be smaller than the actuator with short and fully anchored movable electrode. The pull-down voltage of the beam increases with the initial deflection of the movable electrode and decreases upon partial anchoring of the beam. The behavior of these devices was predicted using a 2D semianalytical model and 3D finite element model. These models correlated well with the experimental results. The movable electrodes with large built-in stress gradient and the beams with large length/width ratio were found to have an initial curvature of polynomial order greater than 2. These devices showed partial snap-down and uncurling of the movable electrode upon application of voltage beyond critical pull-down voltage. Nonuniformity in the built-in stress gradient along the length and surface imperfections on the electrode surfaces aid in partial snap-down of the movable electrode.

Acknowledgments

This material is based upon work supported by the Defense Advanced Research Projects Agency, Defense Sciences Office, DARPA order no. J607 Totally Agile RF Sensor Systems (TASS) issued by DARPA/CMD under contract no. MDA972-00-C-0010. Dr. Dhananjay Bhusari, Brian P. Dusch, and Matthew Morgan of Georgia Tech assisted in fabrication and testing of the electrostatic actuators. The scientific contribution of Dr. Balam A. Willemsen and Dr. Jurgen Musolf of Superconductor Technologies, Inc., is gratefully acknowledged.

Georgia Institute of Technology assisted in meeting the publication costs of this article.

References

1. C. Goldsmith, J. Randall, S. Eshelman, T. H. Lin, D. Denniston, S. Chen, and B. Norvell, *IEEE MTT-S Int. Microwave Symp. Dig.*, **2**, 1141 (1996).
2. J. J. Yao, *J. Micromech. Microeng.*, **10**, R9 (2000).
3. J. D. Zook, D. W. Burns, H. Guckel, J. J. Sniegowski, R. L. Engelstad, and Z. Feng, *Sens. Actuators A*, **A35**, 51 (1992).
4. C. T. C. Nguyen, *Proc. IEEE Ultrason. Symp.*, **1**, 489 (1995).
5. K. Najafi and K. Suzuki, *Thin Solid Films*, **181**, 251 (1989).
6. R. K. Gupta, Ph.D. Thesis, Massachusetts Institute of Technology, Cambridge, MA (1997).
7. H. C. Nathanson, W. E. Newell, R. A. Wickstrom, and J. R. Davis, *IEEE Trans. Electron Devices*, **14**, 117 (1967).
8. A. Dec and K. Suyama, *IEEE Trans. Microwave Theory Tech.*, **46**, 12 (1998).
9. E. K. Chan, K. Garikipati, and R. W. Dutton, *J. Microelectromech. Syst.*, **8**, 208 (1999).
10. E. S. Hung and S. D. Senturia, *J. Microelectromech. Syst.*, **8**, 497 (1999).
11. E. S. Hung and S. D. Senturia, *J. Microelectromech. Syst.*, **8**, 280 (1999).
12. R. Legtenberg, E. Berenschot, M. Elwenspoek, and J. H. Fluitman, *J. Microelectromech. Syst.*, **6**, 234 (1997).
13. S. N. G. Chu, *J. Electrochem. Soc.*, **145**, 3621 (1998).
14. A. K. Chinthakindi, D. Bhusari, B. P. Busch, J. Musolf, B. A. Willemsen, E. Prophet, M. Roberson, and P. A. Kohl, *J. Electrochem. Soc.*, **149**, H139 (2002).
15. M. Schlesinger and M. Paunovic, *Modern Electroplating*, Chap. 4, 4th ed., John Wiley & Sons, New York (2000).